Int. J. Heat Mass Transfer. Vol. 21, pp. 999–1002

0017-9310/78/0999-1002 $02.00/0

SHORTER COMMUNICATIONS

WAVENUMBER DEPENDENCE OF VELOCITY FIELD AMPLITUDE IN CONVECTION ROLLS—THEORY AND EXPERIMENTS

M. DUBOIS,* C. NORMAND† and P. BERGÉ*

(*Received* 15 *September* 1977)

NOMENCLATURE

- a, wavenumber of the roll pattern;
- A_i, coefficient in first order velocity field representation;
- A_{ij}, coefficient in the inhomogeneous part of the second order velocity field representation;
- A_{ijk}, coefficient in the inhomogeneous part of the third order velocity field representation;
- b_i, coefficient in the homogeneous part of the second order velocity field representation;
- B_{ij}, coefficient in the inhomogeneous part of the third order velocity field representation;
- d, depth of the convection layer;
- d_i, coefficient in the homogeneous part of the third order velocity field representation;
- $f(z)$, vertical profile of the first order velocity field representation;
- D, thermal diffusivity;
- p_i, coefficient in the homogeneous part of the second order velocity field representation;
- Pr, Prandtl number $Pr \equiv \nu/D$;
- q_i, coefficient in the homogeneous part of the third order velocity field representation;
- Ra, Rayleigh number;
- Ra_c, critical Rayleigh number;
- Ra_0, Rayleigh number on the neutral curve;
- ΔT, temperature difference applied to the layer;
- $\mathbf{U}$, convective velocity;
- W, vertical component of the convective velocity;
- x, y, coordinates in the horizontal plane;
- z, coordinate in the vertical direction.

Greek symbols

- α, coefficient of thermal expansion;
- $\mathcal{E}$, defined in formula (2a);
- ε, reduced deviation of the Rayleigh number to the critical one $\varepsilon \equiv (Ra - Ra_c)/Ra_c$;
- ν, viscosity;
- θ, temperature perturbation;
- μ_i, coefficient in velocity field representation.

Special symbol

- $\mathcal{L}$, linear operator.

INTRODUCTION

THE PROPERTIES of a fluid layer which undergoes convective motion are characterized by the Rayleigh number Ra which is proportional to the vertical thermal gradient ΔT applied to this layer and by the wavelength Λ of the convective pattern, pattern which consists of straight rolls in the case of the stable structures we observed within our experimental conditions. The critical value Ra_c corresponds to the onset of the convection, its value is $Ra_c = 1707$ when the preferred rolls have the critical wavelength $\Lambda = \Lambda_c \simeq 2d$, d being the depth of the layer. Otherwise we know that for moderately supercritical Rayleigh number $Ra \gtrsim Ra_c$ bidimensional roll structures can exist with wavelength other than Λ_c within a certain range of $\Lambda \neq \Lambda_c$ [1, 2] depending on the Rayleigh number. This problem has been investigated by Busse *et al.* [3, 4], who performed calculations and experiments which results are qualitatively pictured by the "Busse balloon" as drawn on Fig. 1. It represents a curve in the (Ra, a) diagram ($a = 2\pi d/\Lambda$) inside which all the convective bidimensional modes are stable with respect to certain kinds of disturbances.

In previous works [5, 6] we studied quantitatively the spatial behaviour of the velocity field vs Ra for modes of critical wavelength Λ_c, and compared the results with calculations performed using perturbative theory [7, 8]. The aim of this paper is to extend our knowledge of the convective velocity amplitude for convective modes with $\Lambda \neq \Lambda_c$ in comparison with theoretical results.

(A) THEORETICAL RESULTS

The calculation of the velocity field amplitude was performed using a perturbative method. The technical aspects of this procedure, related to the Rayleigh–Bénard problem have been already described by several authors [7, 9, 10]. The theoretical model which describes the physical situation consists in a layer of fluid confined between two horizontal walls of infinite extent, rigid and perfectly conducting. The equations of motion are the Navier–Stokes equations in the Boussinesq approximation where the viscosity ν, the thermal diffusivity D and the expansion coefficient α may be regarded as constant. In the steady state and in the limit of high Prandtl number this set of equations reduces to the usual sixth order differential equation in the variable W, vertical component of

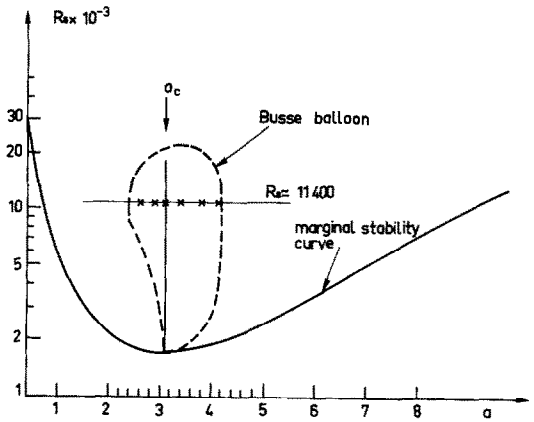

FIG. 1. Stability diagram of convection structures the crosswise points corresponding to the present study. The vertical straight line at a_c represents the previously studied domain [8, 5, 6].

*Service de Physique du Solide et de Résonance Magnétique.

†Service de Physique Théorique.

DPh-, Cen.Saclay, Boite Postale No. 2, 91190 GIF-s/Yvette, France.

the velocity $\mathbf{U}$. In a dimensionless form it expresses as follows

$$(\Delta^3 - Ra\Delta_1)W = -\Delta_1(\mathbf{U}\cdot\mathbf{V})\theta \tag{1a}$$

the scaling factors used for the velocity $\mathbf{U}$, the temperature disturbance θ and the coordinates are respectively D/d, $Ra^{-1}\Delta T$ and d. Δ_1 is the horizontal Laplacian: $\Delta_1 = \partial_x^2 + \partial_y^2$ and the boundary conditions are

$$W = \frac{\partial W}{\partial z} = \Delta^2 W = 0 \quad \text{at} \quad z = \pm\frac{1}{2} \tag{1b}$$

where zz' is the vertical axis.

The equation (1a) is solved by perturbation. But instead of the usual perturbation theory around the critical point of coordinates (Ra_c, a_c) which gives only finite amplitude solutions for rolls pattern of critical wavenumber we are doing a perturbation theory starting from any point $[Ra_0(a), a]$ located on the curve of marginal stability (Fig. 1). This allows to perform calculations for any point (Ra, a) laying in the stable domain situated above the neutral curve. Then the Rayleigh number Ra expands as

$$Ra = Ra_0(a) + \varepsilon Ra^{(1)}(a) + \varepsilon^2 Ra^{(2)}(a) + \varepsilon^3 Ra^{(3)}(a) + \dots \tag{2a}$$

where ε is an arbitrary small parameter.

Analogous expansions hold for $\mathbf{U}$ and θ

$$\mathbf{U} = \varepsilon\mathbf{U}^{(1)}(a) + \varepsilon^2\mathbf{U}^{(2)}(a) + \varepsilon^3\mathbf{U}^{(3)}(a) + \dots \tag{2b}$$

$$\theta = \varepsilon\theta^{(1)}(a) + \varepsilon^2\theta^{(2)}(a) + \varepsilon^3\theta^{(3)}(a) + \dots \tag{2c}$$

Apart from the fact that all parameters $R^{(n)}$, $\mathbf{U}^{(n)}$, $\theta^{(n)}$ are functions of a, the calculation looks like very much as in the standard case and we shall only give a few steps of the calculation. Inserting (2a,b,c) in (1) leads to a set of inhomogeneous differential equations

$$\mathscr{L}[W^{(1)}(a)] = [\Delta^3 - Ra_0(a)\Delta_1]W^{(1)}(a) = 0$$

$$\mathscr{L}[W^{(n)}(a)] = \sum_{p=1}^{n-1} Ra^{(p)}(a)W^{(n-p)}(a) - \Delta_1[(\mathbf{U}^{(p)}(a)\cdot\mathbf{V})\theta^{(n-p)}(a)]$$

The unknown parameters $Ra^{(n)}(a)$ are determined at each order by the existence conditions. Since it appears that all coefficients with an odd superscript are null, the value of ε* is given at the lowest order by

$$\varepsilon = \left(\frac{Ra - Ra_0(a)}{Ra^{(2)}(a)}\right)^{1/2}$$

To describe bidimensional rolls along the xx' direction with yy' axis we are looking for first order solutions of the form

$$W^{(1)}(a) = \cos ax\, f(z)$$

where

$$f(z) = \sum_{i=1}^{3} A_i \cosh \mu_i z \tag{3}$$

with

$$(\mu_i^2 - a^2)^3 + a^2 Ra_0(a) = 0$$

is a general solution of the equation

$$\left[\left(\frac{\partial^2}{\partial z^2} - a^2\right)^3 + a^2 Ra_0(a)\right] f = 0.$$

The second order solution is the sum of a particular inhomogeneous solution and the homogeneous one

$$W^{(2)}(a) = \cos 2ax\left\{\sum_{i=1}^{3}\sum_{j=-3}^{3} A_{ij}^{(2)} \sinh(\mu_i + \mu_j)z - \sum_{i=1}^{3} b_i \sinh p_i z\right\} \tag{4}$$

with

$$(p_i^2 - 4a^2)^3 + 4a^2 Ra_0(a) = 0 \quad \text{and} \quad p_{-i} = -p_i.$$

The RHS of the third order equation provides both terms proportional to $\cos ax$, so-called fundamental mode, and to $\cos 3ax$, so-called third harmonic.

This allows dividing the third order solutions in two parts

$$W^{(3)}(a) = W^{(3,1)}(a) + W^{(3,3)}(a)$$

where the second superscript account for the harmonicity with respect to the x coordinate. We are not interested here in $W^{(3,1)}$ which is difficult to observe experimentally. But $W^{(3,3)}$ which can be measured accurately expresses as

$$W^{(3,3)}(a) = \cos 3ax\left\{\sum_{i=1}^{3}\sum_{j=-3}^{3}\sum_{k=-3}^{3} A_{ijk}^{(3)} \cosh(\mu_i + \mu_j + \mu_k)z + \sum_{i=1}^{3}\sum_{j=-3}^{3} B_{ij}\cosh(\mu_i + p_j)z - \sum_{i=-3}^{3} d_i \cosh q_i z\right\} \tag{5}$$

with

$$(q_i^2 - 9a^2)^3 + 9a^2 Ra_0(a) = 0$$

The coefficients A_i, d_i, b_i being determined successively at each order by the boundary conditions. The results reported here are the maximum value of $W^{(1)}/[Ra^{(2)}]^{1/2}$ and $W^{(3,3)}/[Ra^{(2)}]^{3/2}$ evaluated in the mid height plane of the layer where $z = 0$, so that expressions (3) and (5) take a very simple form. The calculation of these expressions which involves many complex numbers has been carried out on a computer. The results obtained for different values of the wavenumber a are given in Table 1.

(B) EXPERIMENTAL MEASUREMENTS

1. *Introduction*

The experimental conditions were already reported in [5]: we measured the velocity components of a convective fluid confined between two horizontal copper plates and inside a plexiglass rectangular frame; the horizontal extension of the fluid layer is $10 \times 3\,\text{cm}^2$; its depth is $d = 1$ cm. The studied fluid is silicone oil of Prandtl number $Pr = \nu/D \sim 10^3$ where $\nu = 1.18 \pm 0.01$ Stokes at 20°C and D, the thermal diffusivity is $(1.14 \pm 0.04)10^{-3}\,\text{cm}^2\,\text{s}^{-1}$. The local velocity is measured by a laser-Doppler anemometer. The results we give here are related to the vertical component of the velocity W, measured in the mid height plane of the layer.

Table 1.

a	$Ra(a)$	$W_{\max}^{(1)}/[Ra^{(2)}]^{1/2}$	$W_{\max}^{(3,3)}\times 10^5/[Ra^{(2)}]^{3/2}$
2.6	1785.5	0.2580	0.6315
2.8	1735.2	0.2700	0.4509
3	1711.3	0.2806	0.3287
3.2	1709.5	0.2897	0.2428
3.4	1727.0	0.2975	0.1811
3.6	1761.8	0.3039	0.1361
3.8	1812.8	0.3090	0.1028
4	1879.3	0.3129	0.0781

We emphasize the fact that all the convective structures reported in this study consist of straight bidimensional rolls, parallel to $y'y$ axis, so the velocity is independent upon y. Note that $y'y$ axis is parallel to the short side of the frame and $x'x$ parallel to the larger one.

As mentioned in [6], the velocity is periodic vs x and for values of $Ra < 11Ra_c$ we checked that the vertical component W is well described by the following formula

$$W(x,z) = \tilde{W}^1(z)\cos(ax) + \tilde{W}^2(z)\cos(2ax) + \tilde{W}^3(z)\cos(3ax) \tag{6}$$

*In experimental works, the symbol ε is often used as the relative deviation of the Rayleigh number from the critical one as $\varepsilon = \dfrac{Ra - Ra_c}{Ra_c}$.

the origin of the x-axis being taken at a lateral boundary. Indeed, (6) well describes the behaviour of the vertical velocity except in the vertical boundary layers confined in a very narrow region near the lateral boundaries. $W^1(z)$, $\tilde{W}^2(z)$, $\tilde{W}^3(z)$ are the respective Fourier amplitudes of the fundamental, second and third harmonic of the main wavenumber a. The variation of these amplitudes with respect to the wavenumber a are studied by Fourier analysis of the dependences $W(x, z = 0)$ obtained at fixed values of R and a—these analysis are performed by means of a computer program specially designed by Tournarie [11]. As a result of the theory, it appears that $\tilde{W}^{(1)}(z)$ and $\tilde{W}^{(3)}(z)$ are maximum at $z = 0$ $[\tilde{W}^1(0) \equiv \tilde{W}^1_{\max}$ and $\tilde{W}^3_{\max}]$ whereas $\tilde{W}^2(z = 0)$ is null. Furthermore, we have

$$\tilde{W}^1 = \frac{W^{(1)}}{[Ra^{(2)}]^{1/2}} \frac{D}{d} [Ra - Ra_0(a)]^{1/2}$$

and

$$\tilde{W}^3 = \frac{W^{(3,3)}}{[Ra^{(2)}]^{3/2}} \frac{D}{d} [Ra - Ra_0(a)]^{3/2}$$

where $W^{(1)}$ and $W^{(3,3)}$ are the dimensionless coefficients given in Table 1.

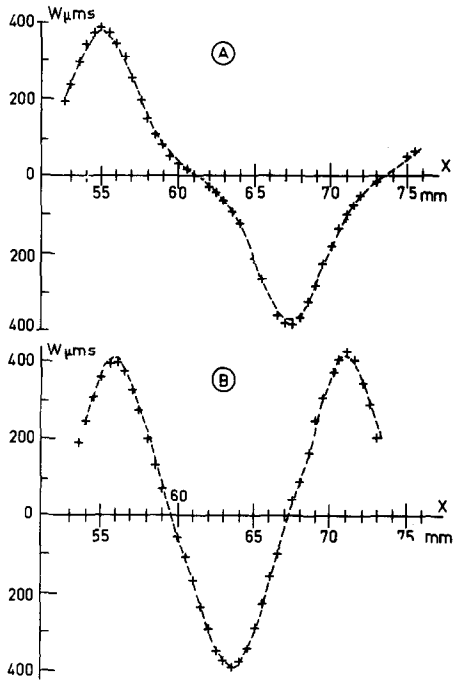

FIG. 2. Spatial dependences of the vertical velocity component W vs x (arbitrary origin) at $Ra \simeq 11\,400$ for two wavelengths. Dashed line represents the computer best fit with curve A: $\Lambda = 24.4$ mm; $a = 2.57$; $\tilde{W}^1 = 294 \pm 2\,\mu m\,s^{-1}$; $\tilde{W}^2 = 3.1 \pm 2\,\mu m\,s^{-1}$; $\tilde{W}^3 = 76{\cdot}5 \pm 2\,\mu m\,s^{-1}$; curve B: $\Lambda = 15.06$ mm; $a = 4.17$; $\tilde{W}^1 = 371 \pm 2\,\mu m\,s^{-1}$; $\tilde{W}^2 = 6.8 \pm 2\,\mu m\,s^{-1}$; $\tilde{W}^3 = 30 \pm 2\,\mu m\,s^{-1}$.

2. *The structures*

In the case of the geometry of the studied layer the different wavelengths have been obtained as follows:

(a) $\Lambda = \Lambda_c$. When the convection is established at a value of ΔT corresponding to $Ra \simeq 3Ra_c$ and if further we gently increase or decrease ΔT, the structure has the critical wavelength $\Lambda = \Lambda_c$, which remains stable in the domain $Ra_c \leqslant Ra \leqslant 11Ra_c$.

(b) $\Lambda < \Lambda_c$. If the layer is suddenly submitted to a large value of ΔT, corresponding to $6Ra_c < Ra < 8Ra_c$, we obtain structures which wavelength is lower than Λ_c.

(c) $\Lambda > \Lambda_c$. If, from a well-established structure, with wavelength Λ_c, we further increase ΔT at values larger than $10\Delta T_c (Ra > 11Ra_c)$ one and further two rolls disappear at the lateral boundaries giving a structure with a wavelength $\Lambda > \Lambda_c$; this new value of Λ can be maintained at lower values of Ra by hysteresis phenomenon [12].

So we have been able to perform measurements for values of Λ ranging from $0.75\Lambda_c$ to $1.22\Lambda_c$ ($2.57 \leqslant a \leqslant 4.17$). We must notice that for $Ra \simeq 11\,400$ at which we have performed the most part of our measurements, we could not obtain other stable convective structures; the observed values of the wavenumber a are extended along the whole width of the Busse balloon, as shown on Fig. 1.

The study of the x-dependences of $W(z = 0)$, see for instance Fig. 2, show that only the fundamental mode and its

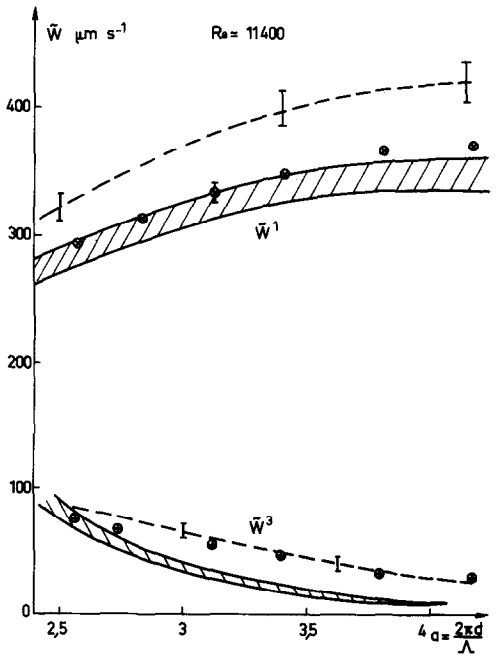

FIG. 3. Amplitudes of the vertical velocity component W vs a for $Ra \sim 11\,400$: ⊗ experimental points corresponding to $\tilde{W}^1$; ⊕ experimental points corresponding to $\tilde{W}^3$; striped areas correspond to the theoretically (Normand *et al.* [7]) computed values including physical uncertainty, dashed lines correspond to the values deduced from Busse's calculations.

Table 2. Measured and calculated velocity amplitudes as a function of the wavenumber a for $Ra = 11\,400$ (W in $\mu m\,s^{-1}$).

	a	2.57	2.84	3.13	3.40	3.80	4.17
Experimental	$\tilde{W}^1$	295±7	314±7	333±7	346±8	367±8	372±8
	$\tilde{W}^3$	76±4	66±4	54±4	46±3	32±3	30±3
Present theory	$\tilde{W}^1$	285	305	321.5	334	346	
	$\tilde{W}^3$	70.7	46.2	29.7	19.6	11.1	
Busse's theory	$\tilde{W}^1$	332	359	382	398	415	
	$\tilde{W}^3$	86	73.4	60.7	49.3	36.7	

third harmonic are needed to account for the behaviour of the vertical velocity component in the midplan of the cell. We have searched for the presence of the fourth and fifth harmonics, but could not establish their presence. We checked also that there was no significant velocity component along $y'y$ i.e. the velocity field was bidimensional. The variations of $\tilde{W}^1$ and $\tilde{W}^3$ with respect to a are given on Fig. 3 and Table 2, for a value of $Ra \simeq 11\,400$. We see that the amplitude of the fundamental mode $\tilde{W}^1$ increases with a, when $\tilde{W}^3$ is decreasing; so the amount of anharmonicity is greater when the wavelength is smaller* (see Fig. 2). From an other point of view, we checked the variation of $\tilde{W}_1$ and $\tilde{W}_3$ with Ra for the structure with $a = 2.57$ and found approximatively the expected power law dependences.

On the Fig. 3 (and Table 2), we give also the velocity amplitudes deduced from the calculated values $W^{(1)}$ and $W^{(3,3)}$. These ones are represented by striped areas, their width being given by the experimental uncertainty on D and Ra. Furthermore, we draw for comparison the values deduced from Busse's results using a Galerkin procedure. The corresponding amplitudes† are not precise for they are obtained from an estimate of parameters taken from a published diagram (uncertainty $\pm 5\%$).

In conclusion, the dependence with respect to a of the measured amplitude of the fundamental mode is well described by the perturbative method. The higher values deduced from Busse's calculations can be mainly explained by the fact that his parameter which gives the fundamental amplitude does not follow the power law in $[(Ra - Ra_c)/Ra_c]^{1/2}$. On the contrary, for the third harmonic amplitudes, the agreement between the experimental points and the values calculated from Busse is very good when the perturbative method gives lower values and a different variation law with a.

Acknowledgement—The authors are grateful to Y. Pomeau for many helpful discussions and valuable suggestions.

*We can notice that the total mass flux carried by convection and deduced from velocity profiles is decreasing when Λ increases.

†There is a misprint in Busse's paper [3] since the values of the coefficients b_{xy} reported in its Fig. 3 are not coherent with the results of the Table 1. They become consistent if we drop a factor π in the value of b_{xy}.

REFERENCES

1. R. Krishnamurti, On the transition to turbulent convection, Part I, *J. Fluid Mech.* **42**, 295–307 (1970).
2. E. L. Koschmieder, Bénard convection, *Adv. Chem. Phys.* **26**, 177–212 (1973).
3. F. H. Busse, On the stability of two-dimensional convection in a layer heated from below, *J. Maths Phys.* **46**, 140–150 (1967).
4. F. H. Busse and J. A. Whitehead, Instabilities of convection rolls in a high Prandtl number fluid, *J. Fluid Mech.* **47**, 305–320 (1971).
5. P. Bergé, Aspects expérimentaux de l'instabilité thermique de Rayleigh–Bénard, *J. Phys. Colloque* $\mathbf{C}_1$, 23–33 (1976).
6. M. Dubois, Effets non linéaires dans le mouvement convectif d'un fluide soumis à l'instabilité de Rayleigh Bénard, *J. Phys. Colloque* $\mathbf{C}_1$, 137–141 (1976).
7. C. Normand, Y. Pomeau and M. G. Velarde, Convective instability: a physicist's approach, *Rev. Mod. Phys.* **49**, 581–624 (1977).
8. M. Dubois and P. Bergé, Experimental study of the velocity field in Rayleigh–Bénard convection, *J. Fluid Mech.* (To be published.)
9. W. Malkus and G. Veronis, Finite amplitude cellular convection, *J. Fluid Mech.* **4**, 225–260 (1958).
10. A. Schlüter, D. Lortz and F. Busse, On the stability of steady finite amplitude convection, *J. Fluid Mech.* **23**, 129–144 (1965).
11. M. Tournarie, Evaluations optimales des inconnues d'un système statistique non linéaire *J. Phys.* **30**, 737–751 (1969).
12. G. E. Willis, J. W. Deardorff and R. C. J. Somerville, Roll-diameter dependence in Rayleigh convection and its effect upon the heat flux, *J. Fluid Mech.* **54**, 351–367 (1972).

Int. J. Heat Mass Transfer. Vol. 21, pp. 1002–1005

0017-9310/78/0701-1002 $02.00/0

A LOCAL SIMILARITY MODEL FOR THE HEAT FLUX EQUATION IN A TURBULENT BOUNDARY LAYER

R. A. ANTONIA
Department of Mechanical Engineering, University of Newcastle, N.S.W. 2308, Australia

and

H. Q. DANH
Department of Mechanical Engineering, University of Sydney, N.S.W. 2006, Australia

(*Received* 22 *April* 1977 *and in revised form* 13 *September* 1977)

NOMENCLATURE

a_1, a_2, a_3, a_0, turbulence structure parameters, assumed constant;
L, length scale defined by equation (2);
l, mixing length $= -\overline{uv}^{1/2}/(\partial U/\partial y)$;
Pr_t, turbulent Prandtl number;
p, turbulent kinematic pressure fluctuation;
q^2, turbulent kinetic energy $(=\overline{u^2}+\overline{v^2}+\overline{w^2})$;
T, difference between local and mean and free stream ambient temperatures;
U, local mean velocity;
u, v, w, velocity fluctuations in x, y and z directions;
$-\overline{uv}$, Reynolds shear stress;
$-\overline{u\theta}$, longitudinal heat flux;
u_τ, friction velocity;
$v\theta$, normal heat flux;
x, y, z, coordinates in longitudinal (streamwise), normal (to wall) and spanwise directions respectively;